JACS
JOURNAL OF THE AMERICAN CHEMICAL SOCIETY
Article
pubs.acs.org/JACS

Effects of Atomic Geometry and Electronic Structure of Platinum Surfaces on Molecular Adsorbates Studied by Gap-Mode SERS

Jian Hu,[†,‡] Masahiro Tanabe,[†] Jun Sato,[†] Kohei Uosaki,[‡,§] and Katsuyoshi Ikeda*[,†,‡,∥]

[†]Division of Chemistry, Graduate School of Science, Hokkaido University, Sapporo 060-0810, Japan
[‡]Global Research Center for Environment and Energy based on Nanomaterials Science (GREEN) and [§]International Center for Materials Nanoarchitectonics (WPI-MANA), National Institute for Materials Science (NIMS), Tsukuba 305-0044, Japan
[∥]Japan Science and Technology Agency, PRESTO, 4-1-8 Honcho, Kawaguchi, Saitama 332-0012, Japan

Supporting Information

ABSTRACT: Surface enhanced Raman scattering (SERS) spectra of organic monolayers were measured on various types of polycrystalline and single crystalline Pt substrates with nanometric or atomic surface features, including heteroepitaxial Pt monolayers, using sphere-plane type nanogap structures. Although atomic geometry and electronic structures of a metal surface significantly influence metal−molecule interactions, such effects are often hindered in conventional SERS measured on a roughened surface because of the spectral information averaging at various adsorption sites. In this study, the use of atomically defined Pt surfaces revealed detailed surface effects; the observed preferential adsorption geometry on each surface was well explained by atomic surface arrangements. The peak shift of the intramolecular vibration in the anchor group was in good agreement with the variation of the d-band center of Pt substrates. Moreover, in electrochemical SERS study the Stark shift of an extramolecular vibrational mode at around 400 cm^{-1}, which is not accessible in infrared absorption spectroscopy, was monitored on an atomically defined heteroepitaxial Pt monolayer electrode.

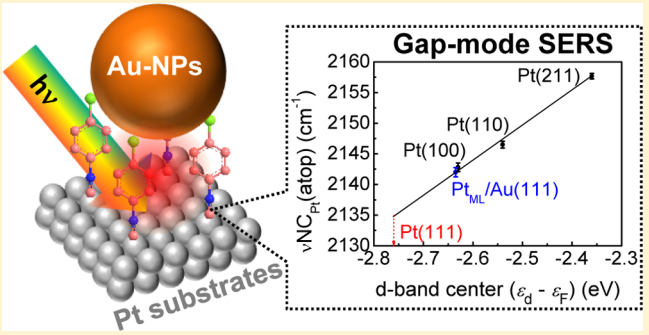

INTRODUCTION

Metal−molecule interactions have been the focus of intense multidisciplinary research, such as catalytic chemistry, materials science, and molecular electronics.[1−3] Vibrational spectroscopy is a powerful tool to study metal−molecule interactions from molecular level information, such as molecular orientations and adsorption geometries. Among various types of the spectroscopic methods, surface-enhanced Raman scattering (SERS) is considered as a promising technique due to its high surface sensitivity and accessibility to low wavenumber region below 1000 cm^{-1}, which gives direct information on metal−molecule interactions, even in IR-opaque media such as aqueous solutions. It is widely accepted that electromagnetic (EM) effect is dominantly responsible for SERS enhancement.[4,5] Since this effect is caused by local field enhancement under excitation of surface plasmons on metal surfaces, conventional SERS measurements have been carried out on electrochemically roughened metal substrates.[6] For getting the larger and reproducible SERS effect, a great deal of efforts have been made in the last few decades to fabricate well-shaped metal nanostructures.[7−10] However, atomic surface features of such SERS-active substrates are normally uncontrollable, which should affect metal−molecule interactions strongly.[11] The exposure of various surface sites on a SERS substrate seriously limits understanding metal−molecule interactions.

Surface control at the atomic scale can be realized by the use of single crystal metal substrates. However, surface plasmons are not directly excited on such a planar surface. The initial successful attempts of SERS detection on single crystalline surfaces were done by an attenuated total reflection (ATR) setup with Otto configuration[12] and tip-enhanced Raman scattering (TERS).[13,14] Under electrochemical conditions, however, the use of these methods is rather difficult due to technical reasons. Moreover, very intense excitation is needed to gain the overall signal intensity in these techniques, which may cause heating up or damage to the sample. Recently, application of sphere-plane type nanogap structures to SERS measurements has been demonstrated on a single crystalline surface of various metals;[15,16] when gold nanoparticles (sphere) are nearly in touch with a single crystalline metal surface (plane), the EM enhancement takes place within the sphere-plane gap (hereinafter, this technique is referred to be as gap-mode SERS). Since a number of SERS-active sites with large enhancement capability, i.e., hot spots,[17,18] are formed on the single crystal surface, one can gain the overall signal intensity using the lower excitation intensity. Using this technique, electrochemical SERS spectra have been clearly observed on single crystalline metal surfaces.[19−22]

Received: February 26, 2014
Published: May 6, 2014

   dx.doi.org/10.1021/ja502008t | J. Am. Chem. Soc. 2014, 136, 10299−10307

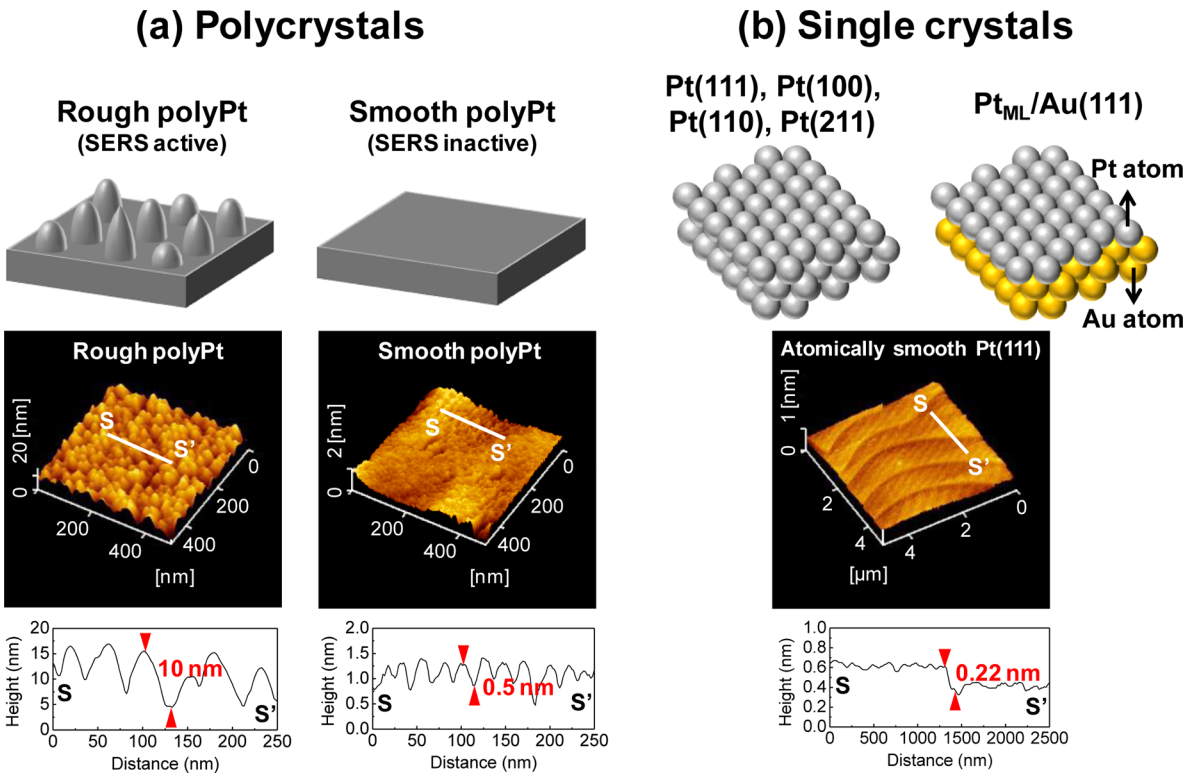

Figure 1. (a) Polycrystalline Pt substrates with nanoscale surface features (Rough polyPt) and with a mirror finished surface (Smooth polyPt), and their AFM topographical images combining with S−S′ line profiles. (b) Face-centered cubic (fcc) single crystalline Pt substrates of various orientations (Pt(111), Pt(100), Pt(110), and Pt(211)), and Pt-epitaxial monolayer formed on Au(111) (Pt$_{ML}$/Au(111)). AFM image shows Pt(111) surface morphology combining with an S−S′ line profile, exhibiting an atomically smooth step-terrace structure with 0.22 nm monatomic steps and ∼1 μm wide terraces.

Metal−molecule interactions are considered to be sensitive to both geometric and electronic surface features. The former stands for the geometric structure of adsorption sites, which may induce steric effects to molecular adsorption. The latter describes the electronic structure of the surface, which is different from the bulk electronic structure. For deeper understanding of the interactions, each contribution should be separately examined on a single crystalline surface. However, when the crystal orientation is altered, both features are changed simultaneously. One frequently utilized method to disentangle the electronic surface features from the geometric one is electrochemical potential tuning of the Fermi level of the metal substrate, which changes the electronic surface features exclusively.[19] The other method is to use epitaxial metal-monolayer formation; the electronic surface features are tuned by interactions between the overlayer metal and the underlying substrate, keeping the atomic surface arrangements invariable.[23,24] It should be emphasized that conventional SERS substrates consist of variety of atomic surface structures, which makes unambiguous analysis of the geometric and electronic substrate effects impossible.

In this work, both geometric and electronic effects on metal−molecule interactions are systematically studied on Pt substrates with various nanometric or atomic surface features by observing gap-mode SERS spectra of self-assembled monolayers (SAMs) of arylisocyanide molecules. For geometric contributions, two different types of surface features are separately examined: nanometric roughness and atomic surface arrangements. To examine nanometric roughness contributions, SERS spectra are compared between an electrochemically roughened SERS-active and a mirror finished SERS-inactive polycrystalline Pt substrate. With respect to atomic arrangement contributions, Pt single crystals of various orientations are thoroughly compared by considering step-terrace structures. For electronic contributions, moreover, SERS spectra are measured on Pt-epitaxial monolayers with and without electrochemical potential control. In the electrochemical SERS, potential-dependent behavior of extramolecular vibrations, which provides direct information on metal−molecule interactions, is demonstrated in conjunction with that of intramolecular vibrations.

■ RESULTS AND DISCUSSION

Figure 1 shows schematic illustrations and atomic force microscope (AFM) topographical images of polycrystalline and single crystalline Pt substrates with various surface features. The detailed preparation methods of these substrates are described in the Methods section. For the polycrystalline substrates, the nanoscale surface features are clearly different between the electrochemically roughened substrate (Rough polyPt) and the mirror finished substrate (Smooth polyPt), as shown in Figure 1a. The former has a large number of bumps with the average height of ∼10 nm, while the latter exhibits a smooth surface with a roughness of ∼0.5 nm. Despite such nanometric geometry features, atomic geometry features and electronic properties are plausibly averaged out on these substrates because various atomic surface sites are exposed on both surfaces. Therefore, one can focus on nanometric geometry effects in comparison with SERS spectra on these surfaces. On the other hand, the single crystalline Pt substrates

dx.doi.org/10.1021/ja502008t | J. Am. Chem. Soc. 2014, 136, 10299−10307

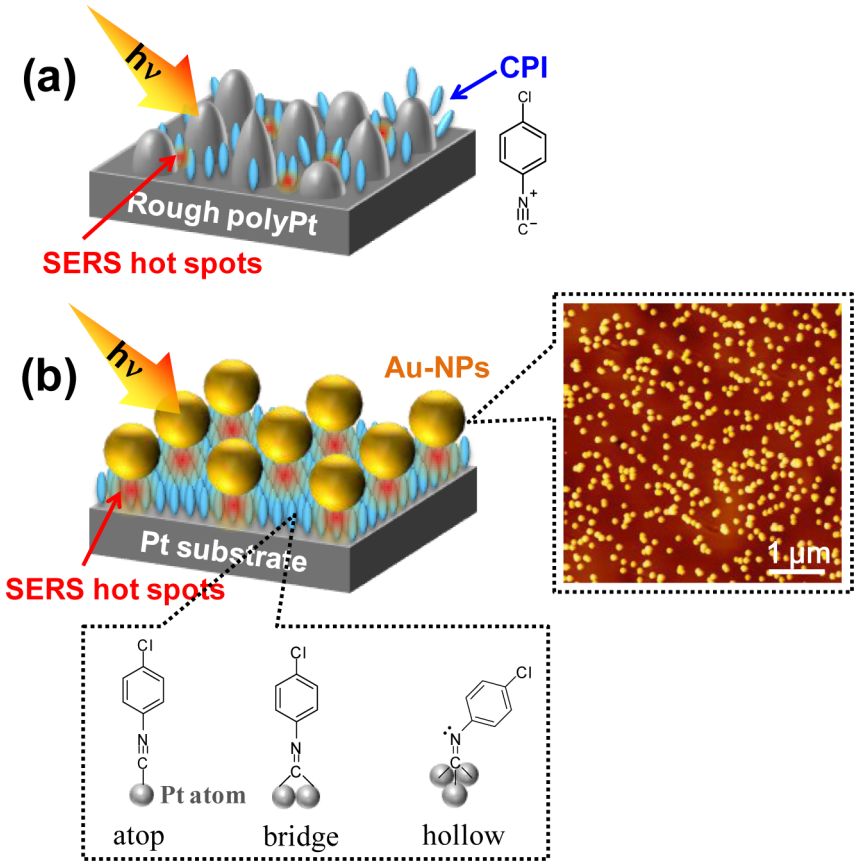

Figure 2. (a) Schematic illustration of conventional SERS system on Rough polyPt. The Pt surface was covered with CPI, where chemical structure is presented in the right-hand side. (b) Schematic illustration of gap-mode SERS system. The right panel shows a typical AFM image of Au-NPs physisorbed on the top of the CPI-SAM. Three possible adsorption geometries of CPI on Pt are shown in the bottom panel.

are known to exhibit characteristic surface features at the atomic scale, which depend on the crystal orientation. In the present study, we employed low index faces of Pt(111), Pt(100), Pt(110), and a high index face of Pt(211) = $3Pt(111)_{terrace}-Pt(100)_{step}$. In addition, Pt monolayer was prepared on the atomically smooth single crystalline Au(111), denoted as $Pt_{ML}/Au(111)$. The AFM topography of Pt(111) clearly indicates an atomically smooth step-terrace structure with ~0.22 nm monatomic steps and ~1 μm wide terraces. These surfaces were exploited to investigate the atomic geometry and/or electronic effects in the absence of the nanometric geometry contributions.

Figure 2 shows schematic illustrations of (a) conventional SERS system and (b) gap-mode SERS system. For both systems, SAMs of 4-chlorophenyl isocyanide (CPI) were formed on the Pt substrates as a model Raman scatterer. In the conventional SERS system, SERS hot spots are created in the valleys among the bumps on Rough polyPt. In the gap-mode SERS system, on the other hand, Au nanoparticles (Au-NPs) with diameter of 50 nm were physisorbed on the top of the CPI-SAMs. We have confirmed that the chemically bound CPI-Pt interfaces remain intact in the presence of the physisorbed Au-NPs,[25,26] which will be again discussed later. The AFM image in the inset of Figure 2b shows that the adsorbed Au-NPs are well-dispersed on the SAM, indicating that the interparticle plasmon hybridization is negligible in the present case.[18,25,26] Therefore, SERS hot spots are created in the gaps between each Au-NP and Pt substrate according to the sphere-plane plasmon hybridization. Among the Pt substrates employed in this work, only the Rough polyPt showed SERS activity in the conventional system. SERS observations on the other substrates were conducted using the gap-mode system.

CPI molecules bind to the Pt substrate with the carbon terminal of the isocyanide (NC) group. Three possible adsorption geometries of CPI on Pt are presented in the bottom panel of Figure 2. Based on the density functional theory (DFT) calculation, one-fold atop and two-fold bridge adsorption are expected to have straight configuration, whereas three-fold hollow adsorption exhibits a notable bent configuration. As shown in the simulated SERS spectra of Figure S1, these configurations can be easily distinguished by the peak position of the intramolecular stretching mode of the NC anchor group, νNC_{Pt}.

Nanometric Geometry Effect: Plasmon-Active Nanostructures. In the conventional SERS method using nanometric surface roughness, Pt is known to be weak SERS active due to its nature of high surface plasmon damping.[11] Even though, six distinctive Raman modes of CPI were observed on the Rough polyPt, as shown in Figure 3a. According to the normal Raman spectrum[15] of free CPI and the DFT calculation results of CPI on Pt shown in Figure S1, the peaks observed at 1090, 1170, 1209, 1571, 1590, and 2140 cm^{-1} are assigned to $\nu C-Cl$, $\delta C-H$, $\nu C-NC$, $\nu C{=}C(ring) + \nu NC_{Pt}(hollow)$, $\nu C{=}C(ring)$, and $\nu NC_{Pt}(atop)$, respectively. Coexistence of the hollow and atop configurations implies that various atomic surface sites are exposed on the surface. Figure 3b shows SERS spectra of CPI on the Smooth polyPt with and without Au-NPs. Before adsorption of Au-NPs (conventional SERS), there

dx.doi.org/10.1021/ja502008t | J. Am. Chem. Soc. 2014, 136, 10299−10307

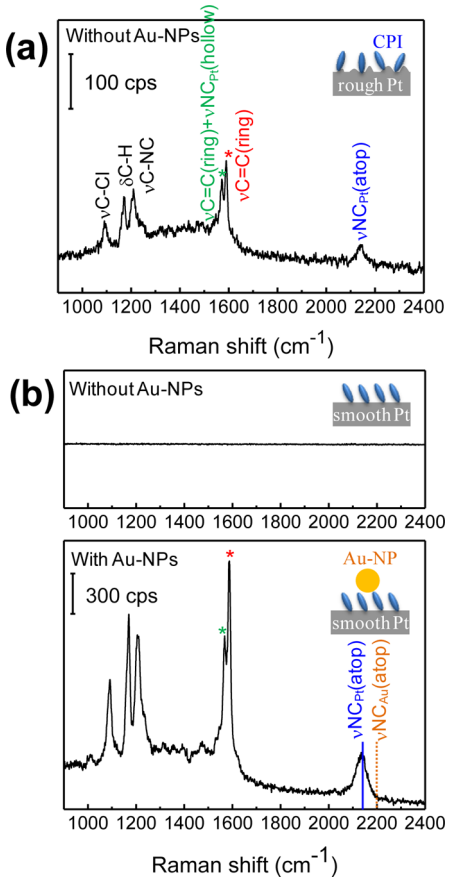

Figure 3. (a) Conventional SERS spectrum of CPI-SAM on Rough polyPt with a roughness of ∼10 nm. (b) Raman spectra of CPI-SAM on Smooth polyPt with a roughness of ∼0.5 nm with and without Au-NPs adsorption.

was no Raman signal observed as expected from the absence of plasmon excitation. After topping Au-NPs on the SAM (gap-mode SERS), the significantly enhanced SERS spectrum was observed much clearer on the smooth surface than on the roughened one. Importantly, there was no obvious difference in the spectral features such as the peak frequency between the conventional and gap-mode SERS spectra; coexistence of the hollow and atop cofigurations was also confirmed on the smooth surface. In addition, the absence of νNC_{Au}, which is generally found at 2190 cm^{-1}, indicates the CPI−Pt interface remains intact in the presence of Au-NPs; transfer of CPI from Pt to Au-NP surfaces was negligible during the SERS experiments. Therefore, the similar spectral appearance between these two types of the Pt substrates demonstrates that the nanoscale roughness does not affect the metal−molecule interaction much, as naturally expected for relatively small molecules.

Atomic Geometry Effect: Crystal Orientation Dependence. Figure 4 shows gap-mode SERS spectra of CPI-SAMs on the atomically defined single crystalline Pt substrates of different orientations. One can clearly see that the spectral features are critically dependent on the crystal orientations. Here, it should be mentioned that the spectral features of gap-mode SERS on single crystalline surfaces are highly reproducible, although the low spectral reproducibility has been the common problem in conventional SERS. According to the peak assignment of νNC_{Pt}, the preferential adsorption geometry of CPI is determined to be the hollow on Pt(111)

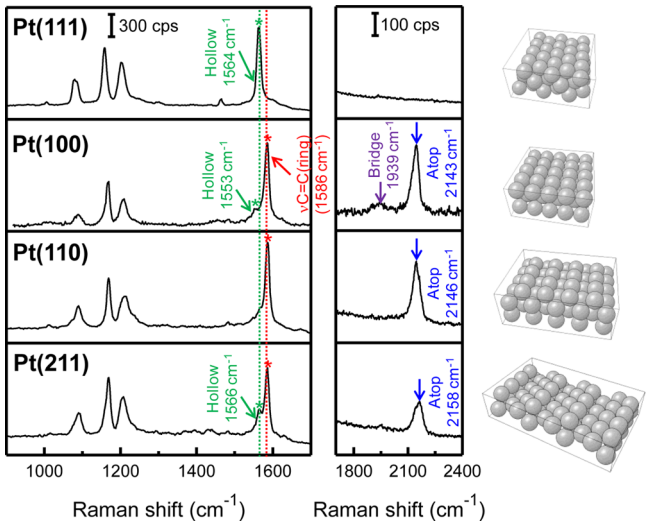

Figure 4. Crystal orientation-dependent gap-mode SERS spectra of CPI-SAMs on various single crystalline substrates of Pt(111), Pt(100), Pt(110), and Pt(211).

and the atop on Pt(110). Coexistence of the hollow and atop is found on Pt(211). Moreover, the quite complicated adsorption is seen on Pt(100), where the dominant atop as well as minor bridge and hollow configurations coexist. The preferential configurations on Pt(111) and Pt(110) are consistent with the geometric features of these surfaces on atomic scale; the three-fold hollow coincides with the hexagonal atomic arrangements of Pt(111), and the atop is expected to be preferable on the atomic row of Pt(110). For Pt(211) = $3Pt(111)_{terrace}$ − $Pt(100)_{step}$, the coexistence of the atop and hollow configurations seems to be reasonable because the atop and hollow adsorptions are geometrically preferable on $(100)_{step}$ and $(111)_{terrace}$, respectively. The most complicated situation on Pt(100) can be also explained from the viewpoint of the atomic geometry effect, which will be discussed later. Clearly, atomic-scale surface sites play a very crucial role in the adsorption geometries. Indeed, SERS spectra on the polycrystalline substrates (Figure 3) can be reproduced as a sum of these spectra on the three low index single crystal faces, meaning that conventional SERS provides only averaged information on the atomic geometry effects on metal−molecule interactions.

Figure 5 shows AFM image of Pt(100), indicating an atomically smooth step-terrace structure with ∼0.22 nm monatomic steps and ∼1 μm wide terraces as well as a large number of ad-islands locating in the middle of the terraces. These ad-islands have already been well investigated by STM observations;[27−29] the right panel in Figure 5 illustrates a ball model of the atomic arrangements on Pt(100) containing one ad-island and one step line. There are predominant $(100)_{terrace}$ sites, $(110)_{step}$ sites on the ad-island edge, and $(111)_{step}$ on the step edge, as indicated by yellow boxes. Taking into account the SERS spectrum on Pt(100), it is considered that the atop, bridge, and hollow configurations are preferable on $(100)_{terrace}$, $(110)_{step}$, and $(111)_{step}$, respectively. The bridge adsorption on the $(110)_{step}$ is different from the atop adsorption observed on Pt(110), which might be due to higher adsorption energy at the ad-island edges, i.e., additional electronic effects. The crystal orientation-dependent gap-mode SERS spectra on various single crystalline faces give a clear picture that atomic-scale surface sites of substrates closely correlate with the adsorption geometries of molecules.

dx.doi.org/10.1021/ja502008t | J. Am. Chem. Soc. 2014, 136, 10299−10307

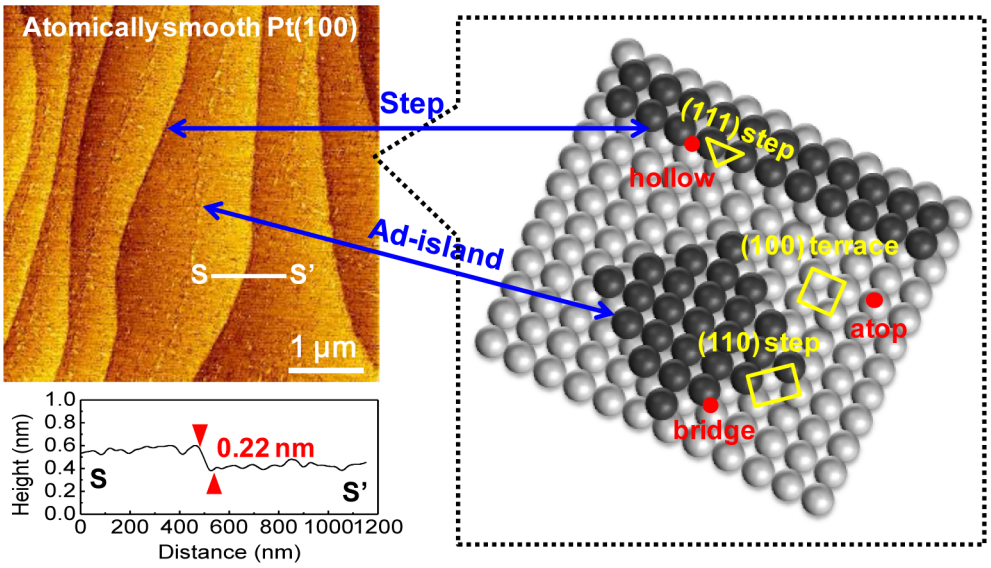

Figure 5. AFM image of Pt(100) measured in air with a scan area of 5 × 5 μm^2. Pt(100) exhibits an atomically smooth step-terrace structure with ~0.22 nm monatomic steps and ~1 μm wide terraces as well as a large number of ad-islands locating in the middle of the terraces. The right panel shows a schematic top view of unreconstructed Pt(100) containing one ad-island and one step line. The yellow boxes present three different atomic surface sites. Three preferential adsorption geometries of CPI at these sites are indicated by red dots.

Atomic Geometry Effect: Metal Monolayers. Epitaxial metal monolayer formation on a foreign metal substrate is recognized as an effective method to tune metal−molecule interactions.[23] Although metal monolayers have been extensively studied in the field of electrocatalysis,[30,31] spectroscopic investigation of molecular adsorbates is still limited on such surfaces. As for the conventional SERS technique, molecular adsorbates on Pt monolayer have been studied on a rough polycrystalline Au substrate by Weaver et al.[32] However, one needs to take into consideration that SERS spectra measured on such surfaces comprise information from various atomic surface sites. Figure 6 shows SERS spectra of CPI-SAMs measured on Pt monolayers with a roughened polycrystalline Au substrate (Pt_{ML}/Rough polyAu) and with a single crystal Au(111) (Pt_{ML}/Au(111)), as well as measured on Au(111). As expected, the spectral appearance is clearly different between

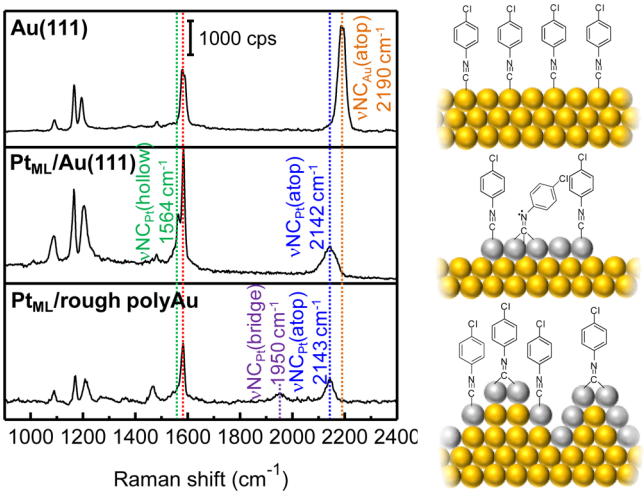

Figure 6. Gap-mode SERS spectra of CPI-SAM on Au(111) and Pt_{ML}/Au(111), and conventional SERS spectrum of CPI-SAM on Pt_{ML}/Rough polyAu.

Pt_{ML}/Rough polyAu and Pt_{ML}/Au(111); the atop and hollow configurations coexist on Pt_{ML}/Au(111) whereas the atop and bridge configurations on Pt_{ML}/Rough polyAu. This result indicates that the atomic surface geometry significantly affects the preferential adsorption configuration of molecular adsorbates. According to the STM studies, the deposited Pt monolayer on Au(111) consists of a large number of two-dimensional interconnected islands.[30,33] Indeed, the present Pt adlayer is not a full covered monolayer, still with 31% Au sites exposed even on Au(111), as shown in Figure S2. Presumably, the atop and hollow configurations on Pt_{ML}/Au(111) are attributed to the adsorption of CPI at the rim and on the terrace of the Pt islands, respectively, and the absence of the hollow adsorption on Pt_{ML}/Rough polyAu is due to the limited area of the (111)-like terrace on the polycrystalline surface. Despite the partial exposure of Au sites at the Pt_{ML}-modified substrates, no νNC_{Au}(atop) was found in the SERS spectra. Such preferential adsorption on Pt sites is not surprising because the NC group interacts with Pt more strongly than Au; we have confirmed that a lower-covered Pt_{ML}/Au(111) presents the νNC_{Au}(atop) peak in SERS spectra (data not shown).

Electronic Effect: Surface Electronic Structures. We have explained the crystal orientation dependence of SERS spectra in Figure 4 on the basis of the atomic geometry effect. Actually, the alternation of the orientation is always accompanied by variation of the electronic effect. When we focus on the atop configuration of CPI, this effect would appear as frequency shifts of νNC_{Pt}(atop) in the crystal orientation-dependent SERS spectra. It is widely accepted that the contribution of surface electronic structures to metal−molecule interactions is well characterized by so-called d-band center (ε_d); the position and width of the d-band of a metal dominantly affect the degree of the interaction, and the d-band center is an indicator of them.[34] Figure 7a shows plots of the peak position of νNC_{Pt}(atop) on the bulk Pt surface, obtained from the data in Figure 4, as a function of the theoretically calculated ε_d (relative to the Fermi level of Pt, ε_F) for each

dx.doi.org/10.1021/ja502008t | J. Am. Chem. Soc. 2014, 136, 10299−10307

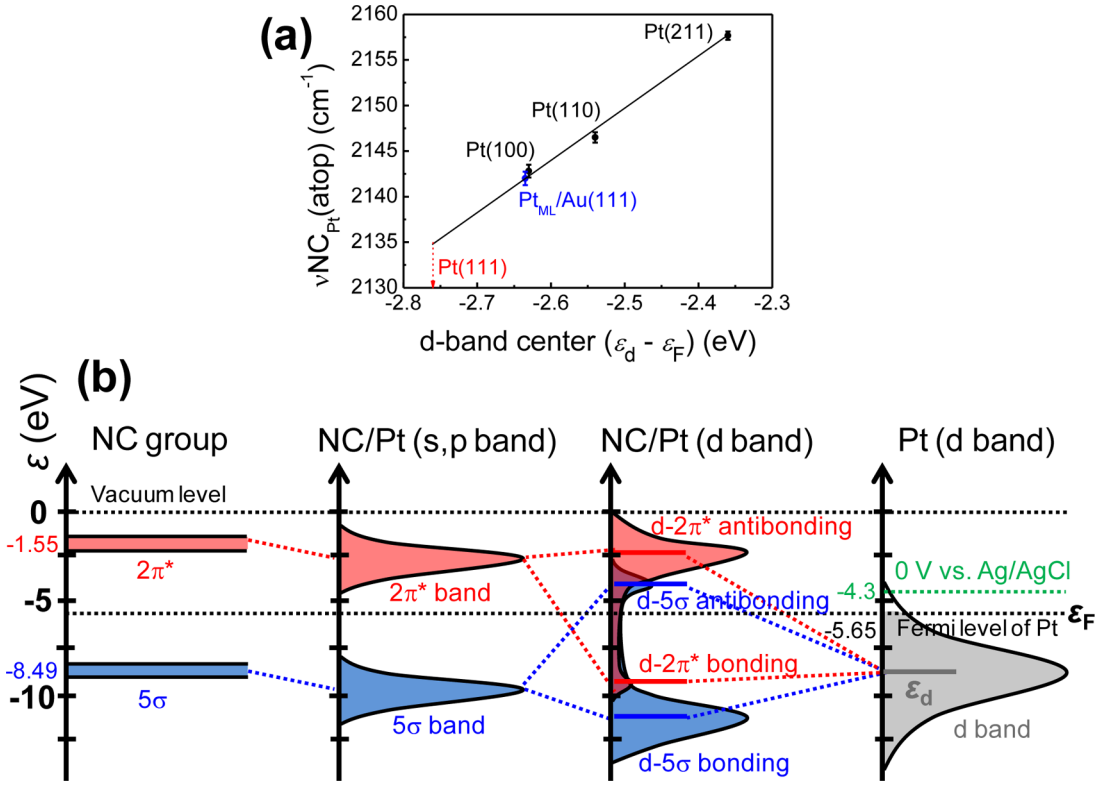

Figure 7. (a) Peak position of νNC_{Pt}(atop) as a function of the d-band center for various single crystalline Pt substrates and Pt_{ML}/Au(111). The linear fitting was conducted among Pt(100), Pt(110), and Pt(211). (b) Energy diagram for CPI adsorbed on a Pt substrate. The molecular orbital notations of 5σ and $2\pi^*$ for NC follow those for the isoelectronic CO.

orientation.[35,36] Clearly, the peak position has a linear relation among Pt(100), Pt(110), and Pt(211), which indicates that the electronic effect is observable using the gap-mode SERS technique.

The stretching frequency of νNC_{Pt} is sensitive to the interaction between NC and Pt, which is illustrated by an energy diagram, as shown in Figure 7b. According to the DFT calculation, the filled 5σ and empty $2\pi^*$ orbitals of the unbound NC group locate below and above the Fermi level of Pt, respectively. (These molecular orbital notations of 5σ and $2\pi^*$ for NC follow those for the isoelectronic CO.) These two frontier orbitals first couple with the sp electrons of Pt, leading to broadening and down shifts in energy. The broadened bands further hybridize with the d-band of Pt to split into the corresponding bonding and antibonding states. Among these hybridized states, the d-5σ antibonding and d-$2\pi^*$ bonding states are responsible for the σ donation and π back-donation, respectively. It is widely accepted that the σ donation strengthens the N−C bond due to the weak antibonding nature of the 5σ orbital, resulting in a blue shift of νNC_{Pt}; on the other hand, the π back-donation weakens the N−C bond due to the strong antibonding nature of the $2\pi^*$ orbital, resulting in a red shift of νNC_{Pt}.[37] As readily rationalized from Figure 7b, the upshift of ε_d enhances the splitting of the hybridized states, resulting in the simultaneous increase in the σ donation and π back-donation,[35,38] which gives rise to the opposite contributions to νNC_{Pt}. In the case of CPI molecules, it is evident that the σ donation dominantly contributes to the bond formation between NC and Pt because all of the νNC_{Pt}(atop) observed here are higher than νNC of the unbound CPI at 2127 cm^{-1}.[15,39] Since ε_d is known to be crystal orientation dependent, the linear increasing relation between the νNC_{Pt}(atop) and ε_d in Figure 7a is readily explained by considering the crystal orientation dependence of the σ donation. Incidentally, this trend is opposite of that for the isoelectronic carbon monoxide (CO) adsorbed on Pt. Since the energy levels of the 5σ and $2\pi^*$ orbitals are different between NC and CO, the degrees of the σ donation and π back-donation are different between them. Consequently, the upshift of ε_d gives rise to a red-shift of νCO_{Pt} due to the dominant contribution from the π back-donation.[40]

For the atop configuration, the Pt_{ML}/Au(111) also showed the peak at 2142 cm^{-1} as shown in Figure 6. According to the linear relation between νNC_{Pt}(atop) and $\varepsilon_d - \varepsilon_F$ for the bulk single crystalline Pt surfaces, the $\varepsilon_d - \varepsilon_F$ for Pt_{ML}/Au(111) was estimated to be −2.64 eV, as shown by one blue dot in Figure 7a. This is clearly different from the theoretical $\varepsilon_d - \varepsilon_F$ for bulk Pt(111) of −2.76 eV, which is shown by the red arrow in the figure. The upshift of the d-band center in Pt_{ML} agrees with the theoretical prediction for a laterally expanded pseudomorphic monolayer by Nørskov et al. although quantitative agreement was not obtained.[41]

Electronic Effect: Electrochemical Potential Dependence. In a specific surface density of states in the NC-Pt system, the degree of the σ donation and π back-donation can be varied by electrochemical potential control of the Fermi level (ε_F) in an electrolyte solution. Although this method is common in conventional SERS on a rough metal surface, it is not on an atomically defined metal surface. Figure 8a shows the potential-dependent gap-mode SERS spectra of CPI-SAMs on Pt_{ML}/Au(111) in 0.1 M $NaClO_4$ solution. To demonstrate the advantage of SERS spectroscopy, the low frequency region below 500 cm^{-1} is also presented here. This region, in which extramolecular vibrations appear, should provide rich informa-

dx.doi.org/10.1021/ja502008t | J. Am. Chem. Soc. 2014, 136, 10299−10307

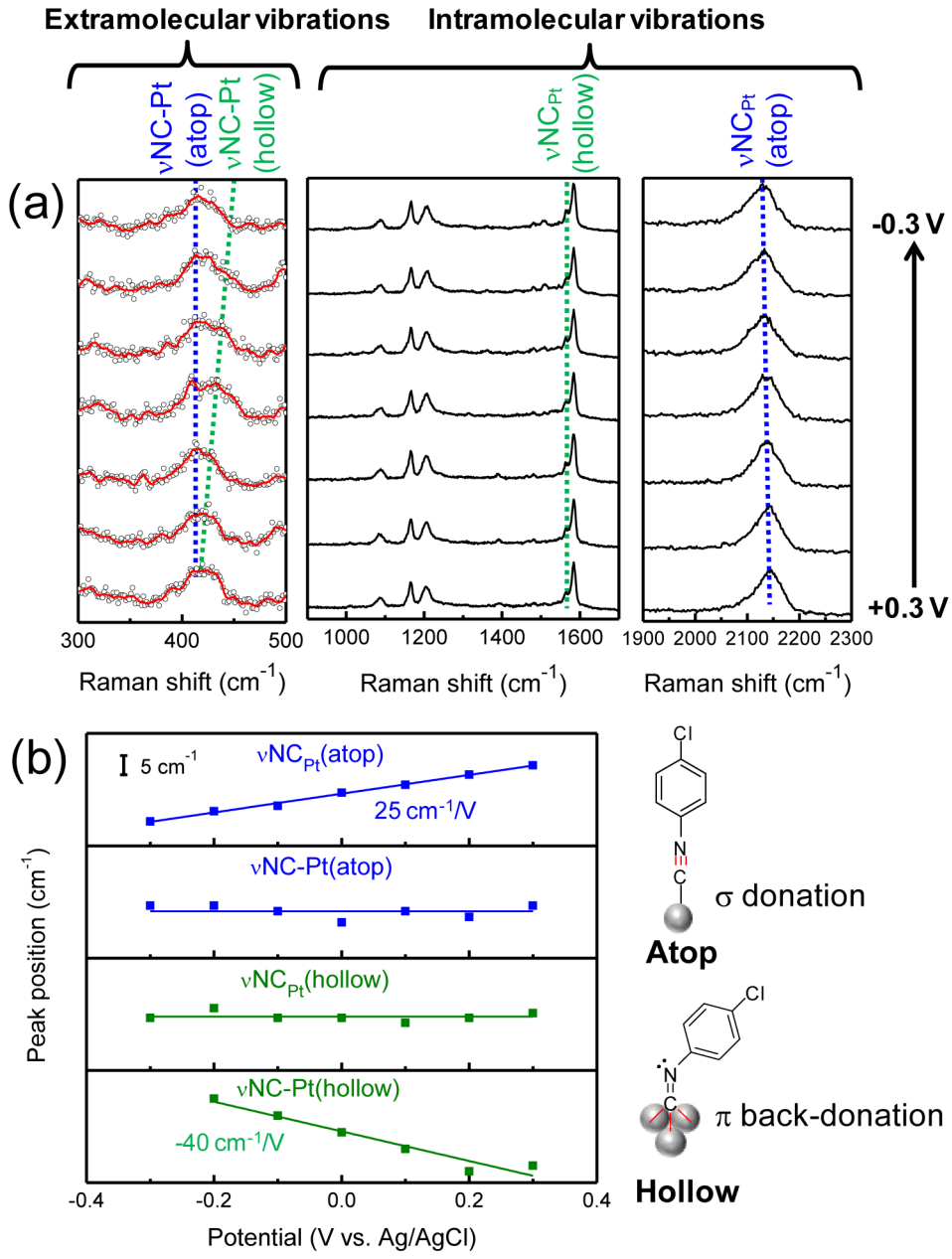

Figure 8. (a) Potential-dependent gap-mode SERS spectra of CPI-SAM on Pt_{ML}/Au(111) in 0.1 M $NaClO_4$ solution, including both extramolecular and intramolecular vibrational modes. (b) Peak positions of the intramolecular νNC_{Pt} and the extramolecular νNC-Pt for both atop and hollow configurations as a function of the electrode potential.

tion on metal−molecule interactions, although IR spectroscopy cannot access it. In the low frequency region, the extramolecular νNC-Pt(hollow) significantly shifts to the high frequency during the potential scan to the negative direction, whereas the νNC-Pt(atop) is almost constant. (The peak assignment can be confirmed in Figure S3, which shows that the νNC-Pt(hollow) on Pt(111) and the νNC-Pt(atop) on Pt(110) appear at 436 and 412 cm^{-1}, respectively, in ambient condition.) In the high frequency region, the intramolecular νNC_{Pt}(atop) shows a notable red shift during the potential scan to the negative direction, so-called positive Stark effect, while the νNC_{Pt}(hollow) remains almost the same. Figure 8b shows the frequencies of these four Raman bands plotted as a function of the applied potential. The intramolecular νNC_{Pt}(atop) responds to the potential variation with a positive Stark slope of 25 cm^{-1}/V, while the extramolecular νNC-Pt(hollow) with a negative Stark slope of −40 cm^{-1}/V.

The electrochemical Stark shift may originate from the electromagnetic effect in the electrical double layer as well as from the electronic effects at the molecule-electrode bonding.[42] In the sphere-plane nanogap system, the former contribution is negligible within the nanogap region,[43,44] where the SERS enhancement takes place. The latter, which is dominant in the present case, is affected by several factors such as the σ donation, π back-donation, and steric repulsion.[45] As shown in Figure 7b, the ε_F will shift up as a scan to negative potentials, which leads to a decrease in the donation from the d-5σ antibonding orbital and an increase in the back-donation to the d-2π* bonding orbital. For the extramolecular νNC-Pt, therefore, the former leads to a red shift while the latter to a blue shift. For the intramolecular νNC_{Pt}, both contributions

dx.doi.org/10.1021/ja502008t | J. Am. Chem. Soc. 2014, 136, 10299−10307

give rise to a red shift of the vibration as already mentioned. In the case of the atop CPI, which is dominantly affected by the σ donation, the red shift of νNC_{Pt}(atop) is expected to be more sensitive to the electrochemical potential than that of νNC-Pt(atop) due to the weak antibonding nature of the 5σ orbital. On the other hand, the hollow adsorption is significantly influenced by the π back-donation because νNC_{Pt}(hollow) is red-shifted from $\nu NC_{unbound}$, which can induce the bent conformation through rehybridization of the NC molecular orbitals. In this conformation, charge localization on the nitrogen atom, i.e., the decrease of the NC bond order, makes the red shift of νNC_{Pt}(hollow) insensitive to the electrochemical variation of the π back-donation, while the blue shift of νNC-Pt(hollow) is significantly induced. Moreover, the coupling with the benzene ring vibration in the νNC_{Pt}(hollow) makes the frequency shift smaller. As a consequence, the observed potential dependence is readily understood from the electrochemical change of ε_F in the energy diagram.

CONCLUSIONS

SERS observations were conducted on atomically defined metal substrates using the sphere-plane type plasmonic nanostructures. The crystal orientation dependence of the SERS spectra revealed the atomic geometry effects on the metal−molecule interactions, which were normally hindered in conventional SERS. The preferential adsorption geometries on each orientation were well explained by considering the atomic surface arrangements. Moreover, the electronic effects induced by crystal orientation, surface metal layer formation, and electrochemical potential tuning were also investigated successfully by gap-mode SERS. So far, most of SERS studies focus on nanometric geometry control of metal substrates to increase the signal enhancement. It is impossible to examine detailed geometric and electronic effects on metal−molecule interactions on these surfaces. As shown in this study, atomic surface control of metal substrates should advance SERS spectroscopy to the next step.

One of the significant advantages of SERS is the accessibility to the low frequency region below 1000 cm^{-1} in aqueous solutions, which is almost impossible for infrared reflection absorption spectroscopy or vibrational sum-frequency generation spectroscopy. Since this region includes rich information on substrate−molecule interactions as extramolecular vibrations, electrochemical SERS observations on an atomically defined electrode should help us to understand the detailed picture of metal−molecule interactions. In this work, we have clearly observed the Stark shift of the extramolecular vibration, νNC-Pt(hollow), on an atomically smooth surface. The correlation of the electrochemical behavior between the extramolecular and intramolecular vibrations of the NC anchor was found to be opposite between the atop and hollow configurations. The gap-mode SERS spectroscopy on single crystals is expected to support technological advancements in various research fields such as electrocatalysis, molecular electronics, and materials science.

METHODS

Preparation of Various Pt Substrates. Various polycrystalline and single crystalline Pt substrates shown in Figure 1 were prepared as follows. The surface morphology of all the substrates were measured using a commercial AFM unit (AFM5100N, Hitachi High-Tech Science Corp., Japan).

Polycrystalline Pt Substrates. A mirror finished smooth polycrystalline Pt substrate (Smooth polyPt) was prepared by successive mechanical polishing of a Pt disk (diameter: 10 mm, thickness: 5 mm) using 3, 1, and 0.25 μm diamond suspensions and 0.05 μm alumina suspension (Buehler, Ltd.). A SERS-active rough polycrystalline Pt substrate (Rough polyPt) was prepared by oxidation−reduction cycle technique. The square waves of 100 Hz with upper and lower switching potentials of 2.4 and −0.2 V vs Ag/AgCl (saturated KCl) reference electrode were applied to the Smooth polyPt in 0.1 M H_2SO_4 solution for 30 min, and then the potential was kept at −0.2 V to reduce the surface oxide layer.

Atomically Smooth Single Crystalline Pt Substrates. A single crystalline Pt bead, ∼3 mm in diameter, was prepared by melting a Pt wire (diameter: 0.8 mm) in a gas flame.[46] After the slow cooling of the Pt bead, four (111) and one (100) facets appear on the top of the bead crystal. SERS measurements on (111) and (100) faces were conducted on these facets. In addition, (110) and (211) crystal faces were determined relative to the crystal orientations of (111) and (100) facets and were prepared by the mechanical polishing method, followed by annealing.

Pt Monolayer Modified Au(111) Surface. The Au(111) polished surface was prepared by mechanical polishing, electropolishing, and hydrogen flame annealing. The Cu underpotential deposition was then conducted on Au(111) in 0.1 M H_2SO_4 + 1 mM $CuSO_4$ solution, by sweeping the potential from +0.6 to +0.06 V at the scan rate of 1 mV/s and holding at +0.06 V for the additional 5 min (see Figure S2). After rinsed with Milli-Q water, the Cu monolayer modified Au(111) was transferred into 0.1 M $HClO_4$ + 5 mM K_2PtCl_4 solution for 5 min to obtain Pt monolayer modified Au(111), Pt_{ML}/Au(111), by surface-limited redox replacement of Cu with Pt.[33]

SAM Formation. All of the substrates except for Rough polyPt and Pt_{ML}/Au(111) were annealed by inductive heating for 30 min and then cooled down in an electrochemical cell with Ar/H_2 flow (Ar:H_2 = 97:3) to obtain a well-ordered reconstructed surface structures. Rough polyPt and Pt_{ML}/Au(111) were not allowed to be subjected to annealing, thus freshly prepared substrates were immediately covered with SAMs. SAM formation was conducted by immersing the substrates into a dichloromethane solution containing 10 mM 4-chlorophenyl isocyanide (CPI, Oakwood Products, Inc.) for 16 h, in an argon-purged glovebox.

Raman Measurements. In conventional SERS, CPI-covered Rough and Smooth polyPt were compared to study nanometric geometry effects. For gap-mode SERS, the CPI-covered Pt substrates were further dipped in a colloidal solution of citrate-reduced Au-NPs (Tanaka Kikinzoku Corp.) with diameter of 50 nm for 2 h so that the Au-NPs were physisorbed on the SAMs. The nanogaps between Au-NPs and Pt substrate act as Raman active sites. Raman scattering signals were monitored with a home-built inverted microscope Raman system with an objective lens (40× , 0.6 N.A.). A He−Ne laser radiation (wavelength of 632.8 nm and intensity of 0.02 mW) was chosen as an excitation light source. The focusing of the linearly polarized He−Ne radiation creates *p*-polarized light, which can excite sphere-plane gap-mode plasmons. Therefore, the SERS enhancement in this system depends on the N.A. of the objective lens. The plasmon resonance peak in the present sphere-plane structures is expected to match the excitation wavelength.[26] The backscattered Raman signals from samples were monitored by a CCD-polychromator system (PIXIS 400B, Princeton Instruments) after Rayleigh scattering light was filtered by an edge filter (LP02−633-RU, Semrock). In electrochemical SERS observations, the substrate potential was controlled in a three-electrode cell filled with Ar-bubbled 0.1 M $NaClO_4$ solution. A platinum coil and Ag/AgCl (saturated KCl) serve as counter and reference electrodes, respectively. The acquisition time is 30 s for all the Raman measurements.

ASSOCIATED CONTENT

Supporting Information

Simulated Raman spectra of CPI adsorption on Pt substrates by DFT calculation. Underpotential deposition of Cu on Au(111)

and cyclic voltammograms for Pt_{ML}/Au(111) and Au(111) in 0.1 M H_2SO_4. Gap-mode SERS spectra of CPI on Pt(110), Pt_{ML}/Au(111), and Pt(111) in the low frequency region. This material is available free of charge via the Internet at http://pubs.acs.org.

AUTHOR INFORMATION

Corresponding Author

kikeda@pchem.sci.hokudai.ac.jp

Notes

The authors declare no competing financial interest.

ACKNOWLEDGMENTS

This research was supported in part by a Grant-in-Aid for Young Scientists (A) (no. 24681018) and a Grant-in-Aid for Exploratory Research (no. 24651126) from Japan Society for the Promotion of Science (JSPS), World Premier International Research Center (WPI) Initiative on Materials Nanoarchitectonics and the Program for Development of Environmental Technology using Nanotechnology of the Ministry of Education, Culture, Sports, Science and Technology (MEXT), Japan.

REFERENCES

(1) Ulman, A. *Chem. Rev.* **1996**, *96*, 1533.
(2) Wold, D. J.; Frisbie, C. D. *J. Am. Chem. Soc.* **2001**, *123*, 5549.
(3) Xu, B.; Tao, N. J. *Science* **2003**, *301*, 1221.
(4) Otto, A.; Mrozek, I.; Grabhorn, H.; Akemann, W. *J. Phys.: Condens. Matter* **1992**, *4*, 1143.
(5) Moskovits, M. *Rev. Mod. Phys.* **1985**, *57*, 783.
(6) Fleischmann, M.; Hendra, P. J.; McQuillan, A. J. *Chem. Phys. Lett.* **1974**, *26*, 163.
(7) Dick, L. A.; McFarland, A. D.; Haynes, C. L.; Van Duyne, R. P. *J. Phys. Chem. B* **2002**, *106*, 853.
(8) Li, W. D.; Ding, F.; Hu, J.; Chou, S. Y. *Opt. Express* **2011**, *19*, 3925.
(9) Abdelsalam, M. E.; Mahajan, S.; Bartlett, P. N.; Baumberg, J. J.; Russell, A. E. *J. Am. Chem. Soc.* **2007**, *129*, 7399.
(10) Jain, P. K.; Huang, W.; El-Sayed, M. A. *Nano Lett.* **2007**, *7*, 2080.
(11) Tian, Z. Q.; Ren, B.; Wu, D. Y. *J. Phys. Chem. B* **2002**, *106*, 9463.
(12) Bruckbauer, A.; Otto, A. *J. Raman. Spectrosc.* **1998**, *29*, 665.
(13) Stöckle, R. M.; Suh, Y. D.; Deckert, V.; Zenobi, R. *Chem. Phys. Lett.* **2000**, *318*, 131.
(14) Pettinger, B.; Ren, B.; Picardi, G.; Schuster, R.; Ertl, G. *Phys. Rev. Lett.* **2004**, *92*, 096101.
(15) Ikeda, K.; Fujimoto, N.; Uehara, H.; Uosaki, K. *Chem. Phys. Lett.* **2008**, *460*, 205.
(16) Li, J. F.; Huang, Y. F.; Ding, Y.; Yang, Z. L.; Li, S. B.; Zhou, Z. S.; Fan, F. R.; Zhang, W.; Zhou, Z. Y.; Wu, D. Y.; Ren, B.; Wang, Z. L.; Tian, Z. Q. *Nature* **2010**, *464*, 392.
(17) Aravind, P. K.; Metiu, H. *J. Phys. Chem.* **1982**, *86*, 5076.
(18) Aravind, P. K.; Metiu, H. *Surf. Sci.* **1983**, *124*, 506.
(19) Ikeda, K.; Suzuki, Shuto.; Uosaki, K. *Nano Lett.* **2011**, *11*, 1716.
(20) Ikeda, K.; Suzuki, S.; Uosaki, K. *J. Am. Chem. Soc.* **2013**, *135*, 17387.
(21) Cui, L.; Liu, B.; Vonlanthen, D.; Mayor, M.; Fu, Y.; Li, J.-F.; Wandlowski, T. *J. Am. Chem. Soc.* **2011**, *133*, 7332.
(22) Butcher, D. P.; Boulos, S. P.; Murphy, C. J.; Ambrosio, R. C.; Gewirth, A. A. *J. Phys. Chem. C* **2012**, *116*, 5128.
(23) Kibler, L. A.; El-Aziz, A. M.; Hoyer, R.; Kolb, D. M. *Angew. Chem., Int. Ed.* **2005**, *44*, 2080.
(24) Naohara, H.; Ye, S.; Uosaki, K. *Electrochim. Acta* **2000**, *45*, 3305.
(25) Ikeda, K.; Sato, J.; Fujimoto, N.; Hayazawa, N.; Kawata, S.; Uosaki, K. *J. Phys. Chem. C* **2009**, *113*, 11816.
(26) Ikeda, K.; Sato, J.; Uosaki, K. *J. Photochem. Photobiol., A* **2011**, *221*, 175.
(27) Rudnev, A. V.; Wandlowski, T. *Russ. J. Electrochem* **2012**, *48*, 259.
(28) Sashikata, K.; Sugata, T.; Sugimasa, M.; Itaya, K. *Langmuir* **1998**, *14*, 2896.
(29) Wakisaka, M.; Yoneyama, T.; Ashizawa, S.; Hyuga, Y.; Ohkanda, T.; Uchida, H.; Watanabe, M. *Phys. Chem. Chem. Phys.* **2013**, *15*, 11038.
(30) Adzic, R. R.; Zhang, J.; Sasaki, K.; Vukmirovic, M. B.; Shao, M.; Wang, J. X.; Nilekar, A. U.; Mavrikakis, M.; Valerio, J. A.; Uribe, F. *Top. Catal.* **2007**, *46*, 249.
(31) Zhang, J.; Vukmirovic, M. B.; Xu, Y.; Mavrikakis, M.; Adzic, R. R. *Angew. Chem., Int. Ed.* **2005**, *44*, 2132.
(32) Park, S.; Yang, P.; Corredor, P.; Weaver, M. J. *J. Am. Chem. Soc.* **2002**, *124*, 2428.
(33) Gokcen, D.; Bae, S. E.; Brankovic, S. R. *J. Electrochem. Soc.* **2010**, *157*, 582.
(34) Hammer, B.; Nørskov, J. K. *Adv. Catal.* **2000**, *45*, 71.
(35) Hammer, B.; Nielsen, O. H.; Nørskov, J. K. *Catal. Lett.* **1997**, *46*, 31.
(36) Stamenkovic, V. R.; Fowler, B.; Mun, B. S.; Wang, G. F.; Ross, P. N.; Lucas, C. A.; Markovic, N. M. *Science* **2007**, *315*, 493.
(37) Treichel, P. M. *Adv. Organomet. Chem.* **1973**, *11*, 21.
(38) Newns, D. M. *Phys. Rev.* **1969**, *178*, 1123.
(39) Kim, N. H.; Kim, K. *J. Phys. Chem. B* **2006**, *110*, 1837.
(40) Lu, C.; Lee, I. C.; Masel, R. I.; Wieckowski, A.; Rice, C. *J. Phys. Chem. A* **2002**, *106*, 3084.
(41) Ruban, A.; Hammer, B.; Stoltze, P.; Skriver, H. L.; Nørskov, J. K. *J. Mol. Catal. A: Chem.* **1997**, *115*, 421.
(42) Lambert, D. K. *Electrochim. Acta* **1996**, *41*, 623.
(43) Chazalviel, J. N.; Allongue, P. *J. Am. Chem. Soc.* **2011**, *133*, 762.
(44) Horswell, S. L.; O'Nei, I. A.; Schiffrin, D. J. *J. Phys. Chem. B* **2003**, *107*, 4844.
(45) Wasileski, S. A.; Koper, M. T.; Weaver, M. J. *J. Phys. Chem. B* **2001**, *105*, 3518.
(46) Clavilier, J.; Faure, R.; Guinet, G.; Durand, R. *J. Electroanal. Chem.* **1980**, *107*, 205.